Optical clearing for photoacoustic lympho- and angiography beyond conventional depth limit *in vivo*

Marina V. Novoselova[a,*], Tatiana O. Abakumova[a], Boris N. Khlebtsov[b], Timofei S. Zatsepin[a,c], Ekaterina N. Lazareva[d], Valery V. Tuchin[d], Vladimir P. Zharov[e], Dmitry A. Gorin[a], Ekaterina I. Galanzha[e]

[a] *Skolkovo Institute of Science and Technology, Moscow, Russia*
[b] *Institute of Biochemistry and Physiology of Plants and Microorganisms, Russia*
[c] *Department of Chemistry, Lomonosov Moscow State University, Moscow, Russia*
[d] *Saratov State University, Saratov, Russia*
[e] *University of Arkansas for Medical Sciences, Little Rock, USA*

ARTICLE INFO

ABSTRACT

Photoacoustic (PA) imaging (PAI) is an emerging powerful tool for noninvasive real-time mapping of blood and lymphatic vessels and lymph nodes *in vivo* to diagnose cancer, lymphedema and other diseases. Among different PAI instruments, commercially available raster-scanning optoacoustic mesoscopy (RSOM) (iThera Medical GmbH., Germany) is useful for high-resolution imaging of different tissues with high potential of clinical translation. However, skin light scattering prevents mapping vessels and nodes deeper than 1–2 mm, that limits diagnostic values of PAI including RSOM. Here we demonstrate that glycerol-based tissue optical clearing (TOC) overcomes this challenge by reducing light scattering that improves RSOM depth penetration. In preclinical model of mouse limb *in vivo*, the replacement of conventional acoustic coupling agents such as water on the mixture of 70 % glycerol and 30 % ultrasound (US) gel resulted in the increase of tissue imaging depth in 1.5–2 times with 3D visualization of vessels with diameter down to 20 μm. To distinguish blood and lymphatic networks, we integrated label-free PA angiography (*i.e.*, imaging of blood vessels), which uses hemoglobin as endogenous contrast agent, with PA lymphography based on labeling of lymphatic vessels with exogenous PA contrast agents. Similar to well-established clinical lymphography, contrast agents were injected in tissue and taken up by lymphatic vessels within a few minutes that provided quick RSOM lymphography. Furthermore, co-injection of PA contrast dye and multilayer nanocomposites as potential low-toxic drug-cargo showed selective prolonged accumulation of nanocomposites in sentinel lymph nodes. Overall, our findings open perspectives for deep and high resolution 3D PA angio- and lymphography, and for PA-guided lymphatic drug delivery using new RSOM & TOC approach.

1. Introduction

Diagnostic imaging of lymphatic vessels and lymph nodes (lymphography) together with surrounded blood vessels (angiography) is relevant for clinical management of many diseases, including cancer and lymphedema [1–3]. Current methods for assessing the vascular and lymphatic systems, such as microscopic computed tomography (micro CT), magnetic resonance imaging (MRI), positron emission tomography (PET) and single photon emission computed tomography (SPECT) provide deep imaging of tissues *in vivo*. However, each of them possesses considerable limitations. For example, CT and MRI often require systemic introduction of high doses of contrast agents that might be toxic for a human [4–7]. High-energy photon imaging, such as PET and SPECT, as well as conventional lymphoscintigraphy require introduction of radioactive tracers that increase health risks for patients and operators [4,5]. Furthermore, prolonged image capturing and post-processing time of these methods make them not optimal for real-time imaging, that is important for monitoring highly dynamic processes

including dissemination of cells, drugs and probes by fast blood and lymph flows. Emerging clinical near-infrared (NIR) fluorescent lymphography is supposed to minimize aforementioned limitations because it uses local injection of contrast agent (e.g. indocyanine green (ICG)) that is less toxic than systemic administration [8–10]. However, ICG-based NIR lymphography allows the efficient imaging of lymphatic vessels, but not blood vessels due to absorbance of ICG fluorescence by hemoglobin.

The reliable alternative for methods described above is photoacoustics [11–18]. Photoacoustic (PA) techniques are based on the non-radiative relaxation of absorbed photons into the heat and then into sound due to a short thermoelastic expansion followed by constriction. PA-based methods are less sensitive to light scattering and auto-fluorescence than fluorescence-based approaches, provide label-free visible and NIR imaging of blood vessels using hemoglobin as endogenous high-contrast PA agent and use low safe-for-human laser energies. This combination of parameters is beyond the capability of current angiographical and lymphographical methods. In preclinical and clinical studies PA methods (*e.g.*, PA tomography, PA mesoscopy, PA spectroscopy and PA flow cytometry) have already demonstrated great promise for advanced noninvasive diagnosis of lymphatic and blood systems through skin *in vivo* [11–14,18–22]. Recently, ICG-based PA imaging (PAI) was successfully used for simultaneous mapping of lymphatic vessels and surrounded veins in a whole forearm and lower leg of patients with lymphedema [23]. Despite these promising results, one of the important limitations of PAI is the imaging depth *in vivo*.

Based on our previous studies [21,24–28] and results from other groups [22, 29–37], this challenge can be overcame by tissue optical clearing (TOC), which is based on the use of optical clearing agents (OCA) with a high refractive index. OCA can diffuse into the tissue and partially replace water. This replacement minimizes the differences in refractive indexes of tissues and extracellular fluids that results in decrease of tissue scattering, especially in skin [38]. This effect leads to strong enhancement of PA signal amplitudes from PA-contrast tissues and fluids (*e.g.*, blood) *in vivo*, that was demonstrated in both preclinical and clinical studies [21,26,28]. However, common TOC diagnostic protocols are based on the pre-treatment with OCA that increase time of a procedure; and commercially available PAI instruments (*e.g.*, iThera Medical GmbH., Germany) still offer use of the water tank or ultrasound (US) gel to achieve acoustic wave coupling between tissue and detector [28]. Taking into account (1) good propagation of acoustic (i.e. PA) signals by OCA solutions and (2) some TOC effect of US gel [38], we suggested that increasing depth of commercial PAI can be achieved without prolongation of detection time by using TOC during PAI procedure (Fig. 1). Here we demonstrated that replacement water in the tank of raster-scanning optoacoustic mesoscope (RSOM; iThera Medical GmbH) by the mixture of OCA and US gel provides one-step PAI procedure with increased imaging depth. As an example, we showed the advantages of RSOM & TOC approach for preclinical lympho- and angiography of a mouse limb *in vivo*.

2. Materials and methods

2.1. Materials

Poly-L-arginine hydrochloride (Mw = 15–70 kDa) (PARG), bovine serum albumin (BSA), fetal bovine serum, silver nitrate (99.99 %), tetrachloroauric acid (> 99 %), sodium borohydrate (96 %), phosphate buffer solution (PBS), hydrochloric acid, calcium chloride dehydrate, anhydrous sodium carbonate, sodium chloride were purchased from Sigma-Aldrich (USA). Dextran sulfate sodium salts (MW = 100 kDa) (DEX), sodium hydroxide (99.8 %), ethylene diamine tetraacetic acid disodium salt (EDTA), hexadecyltrimethylammonium bromide (CTAB, 96 %), isoascorbic acid (IAA, > 99 %) were purchased from Fluka. Sulfo-Cyanine 5 (Cy5) was purchased from Lumiprobe LLC (USA). ICG was purchased from Dynamic Diagnostics (USA). US gel «Aquasonic»

was purchased from Parker laboratories, Inc. (USA), Glycerol (99.4 %) was purchased from «El groups» (Russia). All chemicals were used as received without further purification. Deionized (DI) water (specific resistivity higher than 18.2 MΩ cm) from Milli-Q plus 185 (Millipore) water purification system was used to prepare all solutions.

To calculate the volume fraction of glycerol in the solution, the Gladstone-Dale formula was used [39,40]:

$$f\_Glyc = (n\_Glyc-n\_Water)/(n\_(Pure\ glyc)-n\_Water)*100\ \%, \qquad (1)$$

where nGlyc is the refractive index of the investigated glycerol solution (measured experimentally); nWater is the refractive index of water (measured experimentally); nPure glyc glyc is the refractive index of pure glycerol (value 1.4744 according to GOST 6259-75 [Russian State Standard] at the wavelength of 589 nm, 20 °C).

The refractive index of a solution of glycerol and water was measured on a multiwavelength Abbe refractometer DR-M2/1550 (Atago, Japan) using narrow-band interference filters for wavelengths of 546 nm and 589 nm with an accuracy of ± 0.0002 at 20 °C. The refractive index of the studied glycerol solution was 1.4754 for 546 nm and 1.4736 for 589 nm, water - 1.3343 and 1.331, respectively. The volume fraction of glycerol calculated by the formula (1) in the investigated solution was 99.4 %.

2.2. Preparation of multilayer nanocomposites (MNCs)

MNCs were synthetized using the layer-by-layer assembly method. Specifically, spherical porous vaterite particles with an average diameter of ~3–4 μm were synthesized as we previously reported [41]. As a separate procedure, BSA-ICG solution (1 mL, BSA [0.5 mg/ml]: ICG [0.55 mg/ml], 1:2 [v/v]) was diluted with water (1 mL), mixed with calcium chloride solution (1 M, 0.65 mL) followed by injection of 1 M sodium carbonate (0.65 mL) under vigorous agitation for 1 h. Vaterite particles were isolated by centrifugation (1 min, 3′000*g*) and double washed with DI water (2 ml).

To synthetize gold nanorods (GNRs), seed gold particles were prepared by adding water solution of sodium borohydride (10 mM, 0.6 mL) to a mixed aqueous solution of CTAB (0.1 M, 10 mL) and HAuCl₄ (10 mM, 0.25 mL). For preparation of GNRs with the aspect ratio ~4, solutions of silver nitrate (4 mM, 20 mL), HAuCl₄ (10 mM, 50 mL), IAA (80 mM, 10 mL), HCl (1 M, 10 mL), and gold seed solution from the previous step (10 mL) were sequentially added to CTAB solution (0.1 M, 900 mL) under stirring. The nanorods were grown overnight without stirring at 30 °C. GNRs were separated by centrifugation (12′000*g*, 60 min) and resuspended in water. Final concentration of Au in the sample was 0.5 mM as determined using extinction spectra of Au [42].

MNCs were obtained by sequential adsorption of PARG (0.5 mg/mL in 0.15 M NaCl, 1 mL), DEX (1 mg/mL in 0.15 M NaCl), GNRs (0.75 μg/mL) and ICG (0.55 mg/ml) onto the surface of vaterite particles. Then vaterite cores were dissolved in EDTA solution (0.2 M) resulting in shell MNCs. After each adsorption step, as well as after dissolution of the cores, the suspension of MNCs was purified by centrifugation (1 min, 3000*g*) and double washed with DI water (2 ml). As a result, MNCs were prepared with the following layer structure: (PARG/DEX)(PARG/ICG)(PARG/DEX)(GNR/DEX) and loaded with BSA labeled with ICG. The concentration of MNCs in resulted suspension was measured with counting chamber (*i.e.*, hemocytometer). The measurements of the ζ-potential were performed using a Zetasizer Nano ZS instrument (Malvern Instruments Ltd, UK).

2.3. Phantom measurements

To prepare a phantom, we filled a hollow plastic tube with the solution of a PA contrast agents (MNCs, GNR, ICG, lymphazurin and Cy5, 1 mg/ml) and sealed both ends with parafilm (Fig. S1). RSOM images of all phantoms were obtaines were triplicated for each sampleS. We
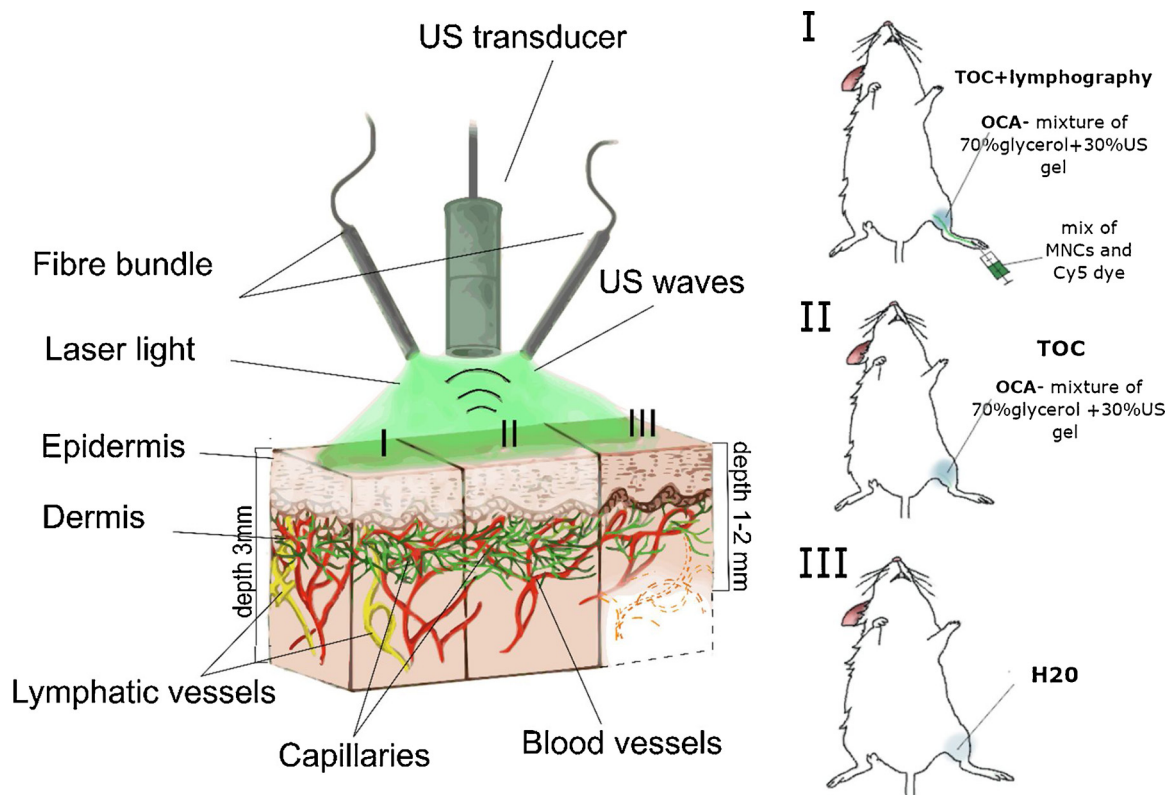
Fig. 1. Schematic of RSOM system and experimental protocol.

avoided dividing detected US frequencies into smaller sub-bands during the reconstruction process. Instead of that, we used mean pixel intensity for analysis of each ROI or phantom.

2.4. PAI of blood and lymphatic vessels in mouse limb in vivo

Experiments *in vivo* were performed in accordance with the ethical standards of the responsible committee on human and animal studies (institutional and national) and with the Helsinki Declaration of 1975, as revised in 2008. The protocols were approved by Animal Ethics Committee at Saratov State Medical University.

Mice (BALB, 4–6 weeks of age, 20–22 g of average weight) were purchased from Andreevka Nursery (Russia). For PAI, we used RSOM in epi-illumination mode. First, animals were anesthetized with isoflurane using standard procedure, and fur in the area of interest was removed with a hair removal cream, (Veet®, Reckitt Benckiser Japan Ltd., Tokyo, Japan). Then mouse was fixed on a heated stage (37 °C) of mesoscope using the protocol provided by iThera Medical GmbH. Fixation and adequate anesthesia were provided over a total time of the experiment. The laser beam was positioned in a middle part of the shaved area of the limb and, then, US transducer was positioned slightly above the skin close to the point of detection. For coupling of acoustic waves, the tiny space between skin and transducer was gently filled by different agents including water, US gel, mix of 30 % US gel and 70 % glycerol, and 99.4 % glycerol. Immediately after this procedure (similar to the conventional RSOM procedure), serial RSOM images of the same area of the limb were obtained every 15 min during 60 min. The scanner illuminated the tissue with a fast monochromatic nanosecond laser (1 ns, 1 kHz, 1 mJ pulse energy at 532 nm). The laser light source was combined with the US detector into a single scan unit using a two-arm fiber bundle. The PA signals were measured with a 50 MHz spherically focused detector (US transducer). The scan was performed in a continuous-discrete mode or using 20 µm raster step. The typical scan took ~5 min of 6×6 mm^2 field. For some images, the acquired signals were divided into 2 frequency bands, 10–33 MHz (low) and 33–99 MHz

(high), color-coded in red (low frequency) and green (high frequency) and reconstructed into combined images. All obtained PA images were analyzed using ImageJ software. Regions of interest (ROIs) were manually selected to quantify the PA signals from blood or lymphatic vessels or phantoms. For vessel analysis, we also estimated the area value of each ROI. A maximum intensity projection (MIP) was used to reconstruct the 3D image. To analyze each line in the MIP, we used ImageJ to convert the MIP image to an 8-bit TIFF file and measured the threshold area in the stacks in the ROI manager. ROIs were used to measure the threshold area on each line.

To visualize lymphatic vessels and test drug-delivery capability, 20 µl of mixture of Cy5 dye (1 mg/mL) and MNC ($2 \cdot 10^8$ particles/mL) solutions were injected in ratio 1:1 into an interdigital space of footpad without touching the detector-illumination unit and moving the mouse.

In selected experiments, the 70 % glycerol (mixture of 99.4 % glycerol and physiological solution, ratio 7/3, v/v) was intradermally injected in the projection of ROI.

2.5. Fluorescent tomography

Before the procedure, animals were anesthetized using isoflurane. The mice were imaged before injection of contrast agents and in 1, 5 and 24 hrs after injection using *in vivo* Imaging Systems (IVIS) Spectrum CT (Xenogen Corp., USA) by using excitation/emission at 640/680 nm for imaging Cy5 and 710-760/810-875 nm for imaging ICG in MNCs. Fluorescence photons were quantified with Living Image software (Xenogen Corp., USA).

2.6. Statistical analysis

Data for each endpoint was analyzed within a group as means and standard errors (SE), then compared. The statistical significance of the data was analyzed using an unpaired Student's *t*-test in GraphPad Prism 8.0. The differences were considered statistically significant if *p*value was ≤ 0.05. To ensure robust and unbiased results, *in vitro*
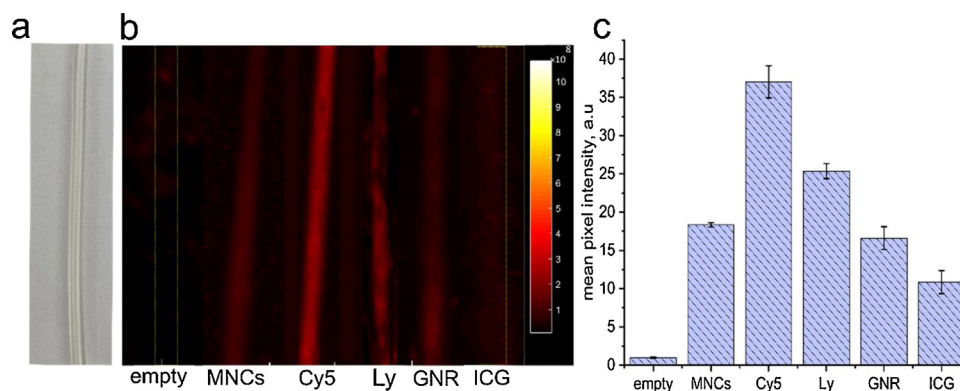
Fig. 2. Vessel phantom *in vitro*. (a) Microscopic optical image of empty phantom. (b) PA images of empty phantom and phantoms filled up by MNCs, Cy5, lymphazurin (Ly); GNR and ICG dye obtained using RSOM. (c) Quantitative analysis of the detected PA signal from different phantoms.

measurements were triplicated, and *in vivo* studies include 5 mice per an experiment.

3. Results and discussion

3.1. Selection of lymphographic PA contrast agents using vessel phantoms

Visualization of PA-transparent lymphatic system with the RSOM requires injection of exogenous PA contrast agents. Physiology of initial lymphatic vessels and one-way lymph flow provide quick (within minutes) and efficient uptake of dyes and nanoparticles and transporting them to the nearest (*i.e.*, sentinel) lymph nodes after local injection into a tissue of interest. This natural lymphatic function is widely used for mapping of lymphatic system (lymphography) in preclinical research and clinical diagnosis.

To optimize PA lymphography with RSOM, we tested various PA contrast agents using a lymphatic vessel phantom, which represented a tube with PA transparent walls (Fig. 2a, **S1**). The spectrum of PA contrast agents included: (1) clinically-approved ICG ($\lambda_{Ex/Em} = 780/800$ nm) and lymphazurin ($\lambda_{Ex/Em} = 650/680$ nm), (2) Cy5 dye ($\lambda_{Ex/Em} = 649/670$ nm), and (3) low toxic GNRs (maximum absorption at 820 nm and smaller peak at 532 nm). Among others, the advantage of ICG and Cy5 is that both of them can be used simultaneously for PAI (RSOM, 532-nm laser) and fluorescent tomography (IVIS). RSOM images of the phantom tubes were obtained before and after filling the tubes with each contrast agent to exclude initial (background) signal. As expected, the strongest PA contrast was observed for Cy5 dye (Fig. 2b,c), while the signal from ICG and GNRs was lower. In order to assess feasibility of RSOM to monitor lymphatic drug delivery with PA-contrast cargos, we also explored MNCs. Our recent studies showed that MNCs, containing layers of ICG and GNRs are promising candidates as PA contrast drug cargos due to their low toxicity and efficacy of intracellular uptake [43,44]. Here we obtained that phantom with MNCs can be robustly detected by RSOM instrument (Fig. 2b). However, the intensity of PA signal was relatively low due to non-optimal wavelength of the existing RSOM to detect ICG. Further using of multi-wavelength RSOM and other PAI technological platforms could optimize imaging and resolve this problem. Nevertheless, the important conclusion from our pilot measurements is that RSOM can be used for high resolution PA imaging of lymphatic vessels.

3.2. Integration of lymphography and angiography with high resolution 3D-PAI in vivo

In our *in vivo* study, we optimized PAI for the mouse limb as a clinically relevant model (Fig. 3a) [45]. First, PAI of the mouse limb blood vessels was obtained using RSOM protocol with water as a conventional coupling medium between the PA transducer and skin. Since

hemoglobin has a high absorption at 532 nm, we imaged blood vessels in a label-free manner. Scanning was performed in a continuous, discrete mode for a 6×6 mm^2 field. Usually, the conventional through-skin RSOM imaging provides well-satisfied 3D mapping of blood vessels at the depth of 0.7–1.3 mm (Fig. 3b). This distance also includes the space between transducer and skin (0.2-0.3 mm), so real imaging depth was only ~1 mm from skin surface. In this area, the post-processing analysis provided distinguishing large and small vessels by frequency and color-coding them by red (large vessels) and green (small vessels) (Fig. 3c). Notably, blood vascular network of healthy mice was not significantly changed over 60 min of RSOM monitoring (Fig. S2).

In contrast to blood vessels, lymphatic vessels and nodes are PA transparent and their mapping requires introduction of contrast agents. Based on the results of our phantom study, we have chosen Cy5 dye as PA contrast agent for RSOM lymphography. Similar to clinical lymphography [46], we injected dye solution in tissue near and proximal of the detection area. The injection was carefully performed without touching the detector-illumination unit and moving the mouse, so that the images obtained before injection can serve as valid controls. The PA signal was quantified by differential image analysis before and after dye administration, that resulted in defining lymphatic vessels with diameter as low as 20 μm in 5 min after injection. Using post-processing analysis, lymphatic vessels were color-coded by blue in images (Fig. 3d and e). Taken together with blood mapping, PAI allowed us to determine sizes and structural interrelationship between lymphatic and blood vessels in the studied area of the tissue in a living animal. We made additional efforts to confirm lymphatic uptake of the Cy5 dye by independent fluorescent imaging. Using fluorescent tomography in the mode of fluorescence and spectral separation, we were able to identify injection site and sentinel (the nearest to injection site) and other lymph node(s) (Fig. 3f, S3).

A number of studies have indicated that lymphatic system provides advanced delivery path for therapeutic molecules, such as anticancer and anti-HIV-1 drugs that can result in their sustained targeted release into a tissue of interest such as lymph nodes [3]. As a potential low-toxic drug cargo, we explored MNC delivery into lymphatic system. Since control of lymphatic drug cargo delivery requires (1) lymphography to map lymphatic vessels and nodes; and (2) defining accumulation of cargos in lymphatic system, mainly, in lymph nodes, we co-injected Cy5 dye and MNCs in the footpad. First, we monitored 60-min local kinetics of these agents in limb tissue using RSOM. In a few minutes after injection, we received well-defined lymphatic vessels of the limb in the RSOM images (*i.e.*, PA Cy5-dye lymphography) that was likely associated with lymphatic uptake of Cy5 dye because small molecules of Cy5 dye spread much faster across the tissues and lymphatic system in comparison to larger MNCs. After RSOM imaging, pharmacokinetics of both contrast agents in a whole mouse body was obtained for 24 h with fluorescent IVIS imaging (Fig. S3). The different sets of
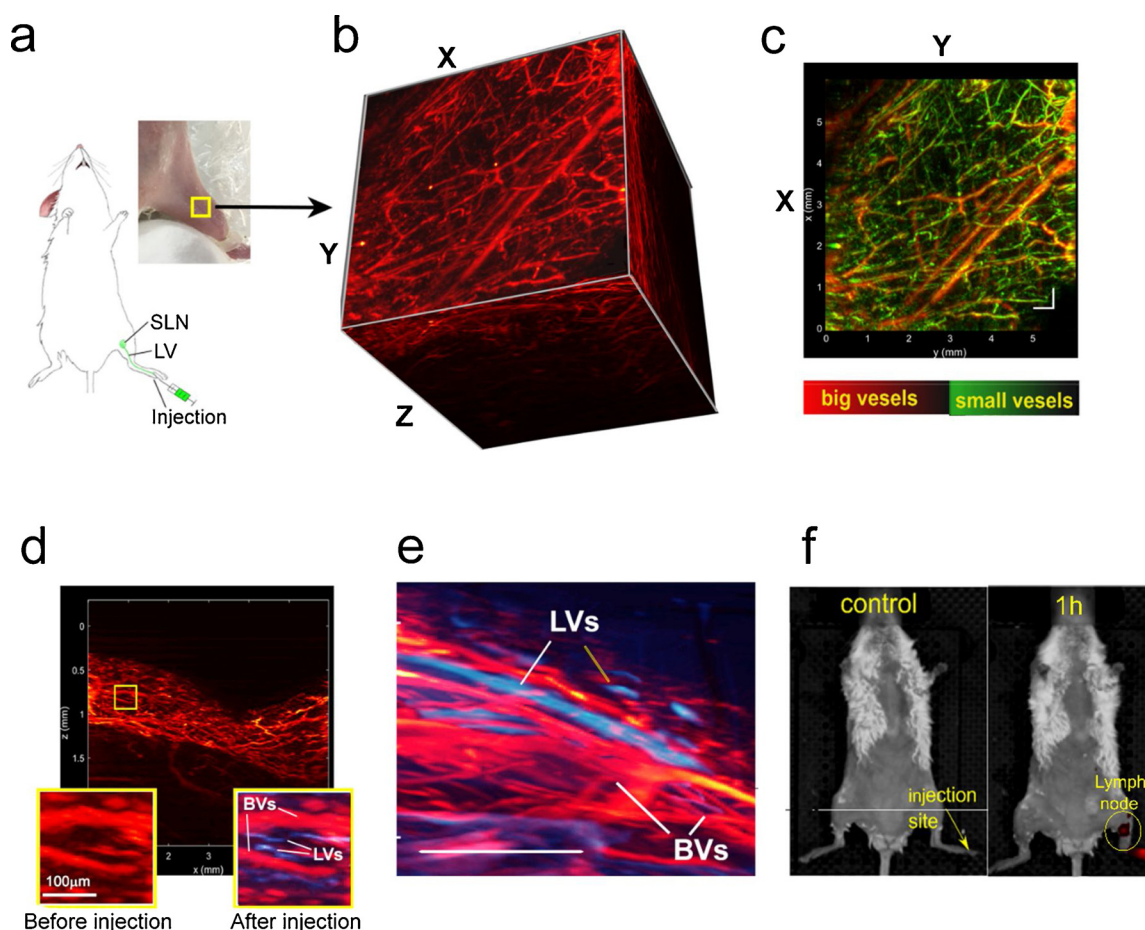
Fig. 3. 3D high resolution PA lymphography + angiography of mouse limb *in vivo*. (a) Scheme of the experiment. (b) 3D reconstruction of RSOM imaging of blood vessels of the mouse limb obtained by using water as a coupling medium. (c) XY scan of the same region as presented in panel "b" with color-coded distinguishing of blood vessels by size: red color = low frequencies (large structures); green color = high frequencies (small structures); yellow color = overlay. (d, e) Integrated images of lymphatic vessels (LVs; blue color) and blood vessels (BVs; red color) after local injection of Cy5 dye (d; XZ scan) and lymphazurin (e). (f) Fluorescence IVIS tomography of a whole mouse before (left) and after (right) footpad injection of mixture of MNCs and Cy5 dye demonstrating accumulation of MNCs (dark-red spot) in the area of a sentinel lymph node in 1 h post-injection; $\lambda_{Ex/Em}$ = 780/800 nm, which is optimal for detection of ICG in MNCs. Scale bar in b–e = 0.5 mm.

excitation/emission filters (excitation 640 / emission 680 nm for Cy5 dye and excitation 780 / emission 800 nm for MNCs) were used to separate fluorescence of Cy5 from fluorescence of MNCs. As expected, Cy5 dye was quickly transported by lymphatic system, entered gastrointestinal tract in 1 h after injection (Fig. S3a, left) and continued to accumulate there during next few hours (Fig. S3a, middle). In 24 h, dye was excreted from organism that was confirmed by the absence of detectable fluorescence signals (Fig. S3a, right). In contrast, MNCs were accumulated only in the areas of local lymph nodes in 1 h after injection (Figs. 3f and S3b, left). In 5 h, fluorescent brightness of lymph node area was enhanced that was likely associated with increased MNC concentration in lymph nodes (Fig. S3b, middle). Simultaneously, some MNCs were spread to gastrointestinal organs and accumulated there in 24 h (Fig. S3b, right).

Thus, for the first time to our knowledge, we demonstrated the feasibility of MNCs to serve as cargos for the targeted delivery of drugs into lymph nodes. The success of this pilot study together with the low toxicity of MNCs [41] provides an exciting potential for using MNCs for lymphatic drug delivery. Furthermore, the beneficiary approach of co-injection of lymphographic contrast agents and drug cargoes would allow using of PAI to control drug delivery and its targeted release *in vivo*.

3.3. Using OCA for acoustic coupling and optical clearing

Despite aforementioned advantages of RSOM for lympho- and angiography, the poor depth might limit its further clinical applications. Here we explored the new advanced approach to integrate PAI and TOC (RSOM & TOC) to increase the depth of PAI. Among various OCA agents, glycerol demonstrated good TOC efficiency and prolonged effective time. Glycerol is widely used in medicine and cosmetics [47]. Since FDA approved glycerol use in cosmetic products for human skin softening, clinical translation of topical application of glycerol on a skin for PA imaging looks highly realistic. This fact prompted us to choose glycerol as an OCA to reduce skin light scattering [21,25–29,36]. Based on our previous experience [25], the best TOC *in vivo* was achieved after intradermal injection of the glycerol. Here, 70 % glycerol solution (at room temperature) was intradermally injected into the area of RSOM imaging in mouse limb. The procedure was performed without any movements, while the detector was raised up and returned to initial position after injection. The 3D PAI after glycerol introduction showed significant elevation of the PA signal at all detected frequencies that significantly improved visualization of both small and large vessels. As shown in Fig. 4a, the depth of resolved angiography was increased in 3–4 times. Furthermore, we observed interesting dynamics in PAI. In 5–15 min after glycerol injection, the main effect was associated with better imaging of the surface vascular network, predominantly small (green) vessels (Fig. 4b, c). With the time elapsed, glycerol diffusion
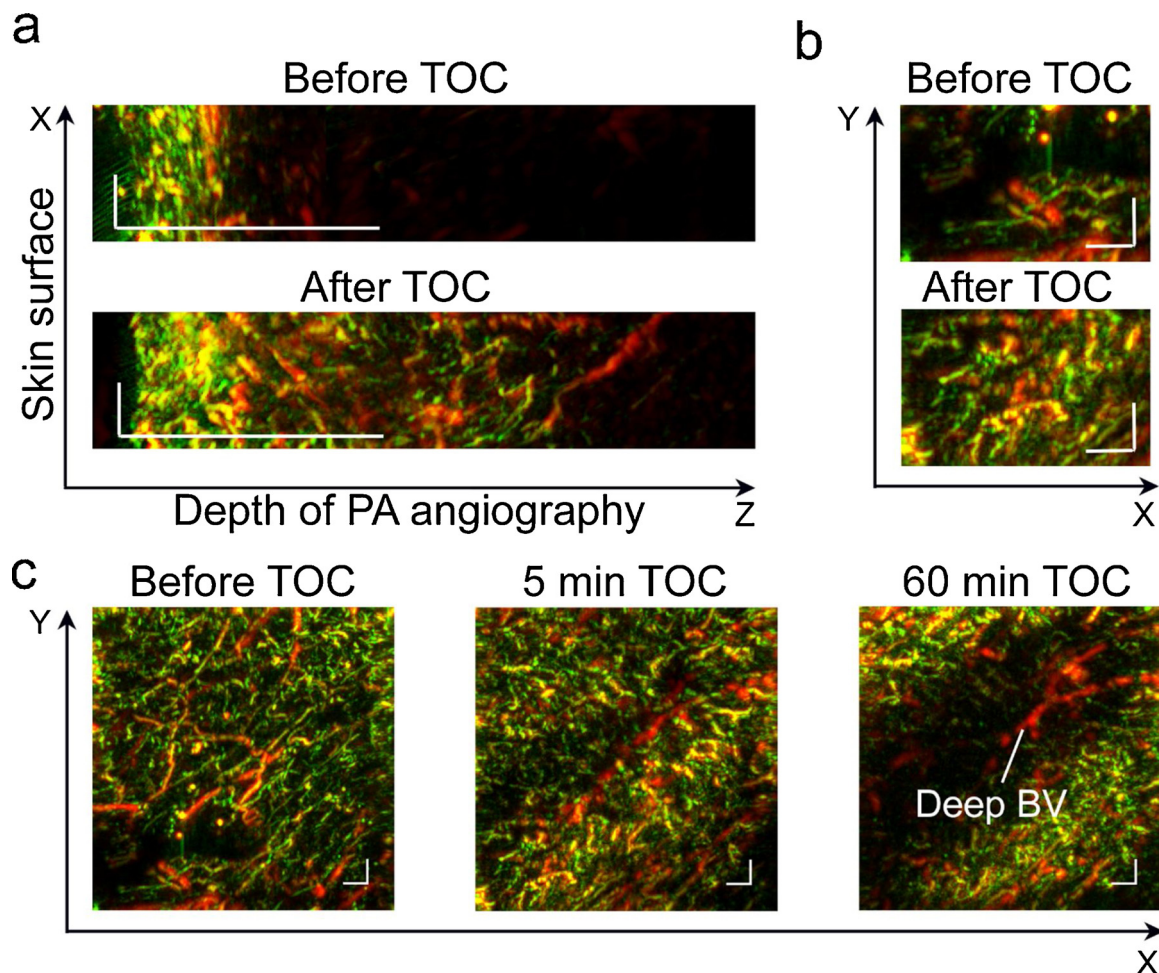
Fig. 4. RSOM imaging and injectable TOC of mouse limb *in vivo*. (a) Increasing depth of detectable blood vessels in XZ scan in 5 min after intradermal injection of 70 % glycerol. (b, c) Effects of injectable TOC on RSOM imaging of the same limb area (XY scans) over 60 min of monitoring: conventional RSOM images of vessels before TOC; improvement in mapping of superficial small vessels in 5 min after glycerol injection due to skin clearing (bottom in "b" and middle in "c") and "open a window" for imaging of deep and large vessels in 60 min after injection as a result of double clearing of skin and superficial vessels (right in "c"). Scale bar = 0.5 mm.

lead to temporal invisibility of superficial vessels in PAI, that allowed imaging of relatively deep vessels, which were stealth before or just after glycerol injection (Figs. 4b,c, S4). It is important for *in vivo* application, that glycerol-induced "disappearance" of superficial small vessels was temporal (minutes after injection), reversible and local (a few mm² area). The presumable mechanism of this phenomenon involves the slowing/stopping of local blood flow and optical clearing of blood cells inside the vessels. This effect of glycerol was previously described for arterioles, venules and capillaries [45], and its usefulness was suggested for improving laser surgery. Here we demonstrated that skin optical clearing in combination with reversible disappearance of superficial vessels open opportunity for high-resolution RSOM to image relatively deep and large blood vessels with no/minimal distortions. However, despite promises of injectable TOC for preclinical studies and its reversibility, the aforementioned changes of blood flow require further careful studies before this approach might be recommended for clinical translation.

To pursuit translation of RSOM & TOC approach to clinic, we tested TOC that includes non-injectable topical application of OCA on the skin surface as a safer method for human. To simplify and shorten PAI protocol with TOC, we used OCA instead of conventional coupling media (*e.g.*, water and US gel). To compare RSOM & TOC and RSOM alone, serial RSOM images of the same area of mouse limb were obtained over the time of 60 min using two conventional coupling media (water and US gel) and two OCA coupling media (pure glycerol and mixture of glycerol and US gel). In groups of mice with RSOM & TOC, each animal before OCA application received a conventional image using water that served as individual controls (Fig. 5).

As expected, we did not obtained significant changes in RSOM images of mouse limb vessels during 60-min application of water (Figs. 5a, S2). In the second group of mice, we replaced water by commercial and clinically-approved US gel that contains some amount of OCA. Serial RSOM images showed a slight improvement in image quality and a small increase in penetration depth (Figs. 5a, S5). The application of pure glycerol also did not provide significant improvements (Figs. 5a, S6). Finally, we used a mixture of glycerol and an US gel. Since the best TOC efficacy was reported for 70 % glycerol solution [48,49], our mixture ratio of glycerol to US gel was 7:3 (v/v). By naked eye, this OCA made skin slightly transparent with better visualization of superficial blood vessels (Fig. S7). In RSOM, significant increasing of imaging depth was obtained in 5 min after topical application of glycerol with US gel. (Figs. 5b, S8). Serial images during 60 min demonstrated that RSOM & TOC provided 1.5–2 -time deeper angiography than standard RSOM. The analysis of volume of 3D objects indicated the improvement of both large and small vessel visualization. The best results of RSOM & TOC were obtained in 5–45 min interval after initial application of the mixture of glycerol and US gel on the skin (Figs. 5a, S8).
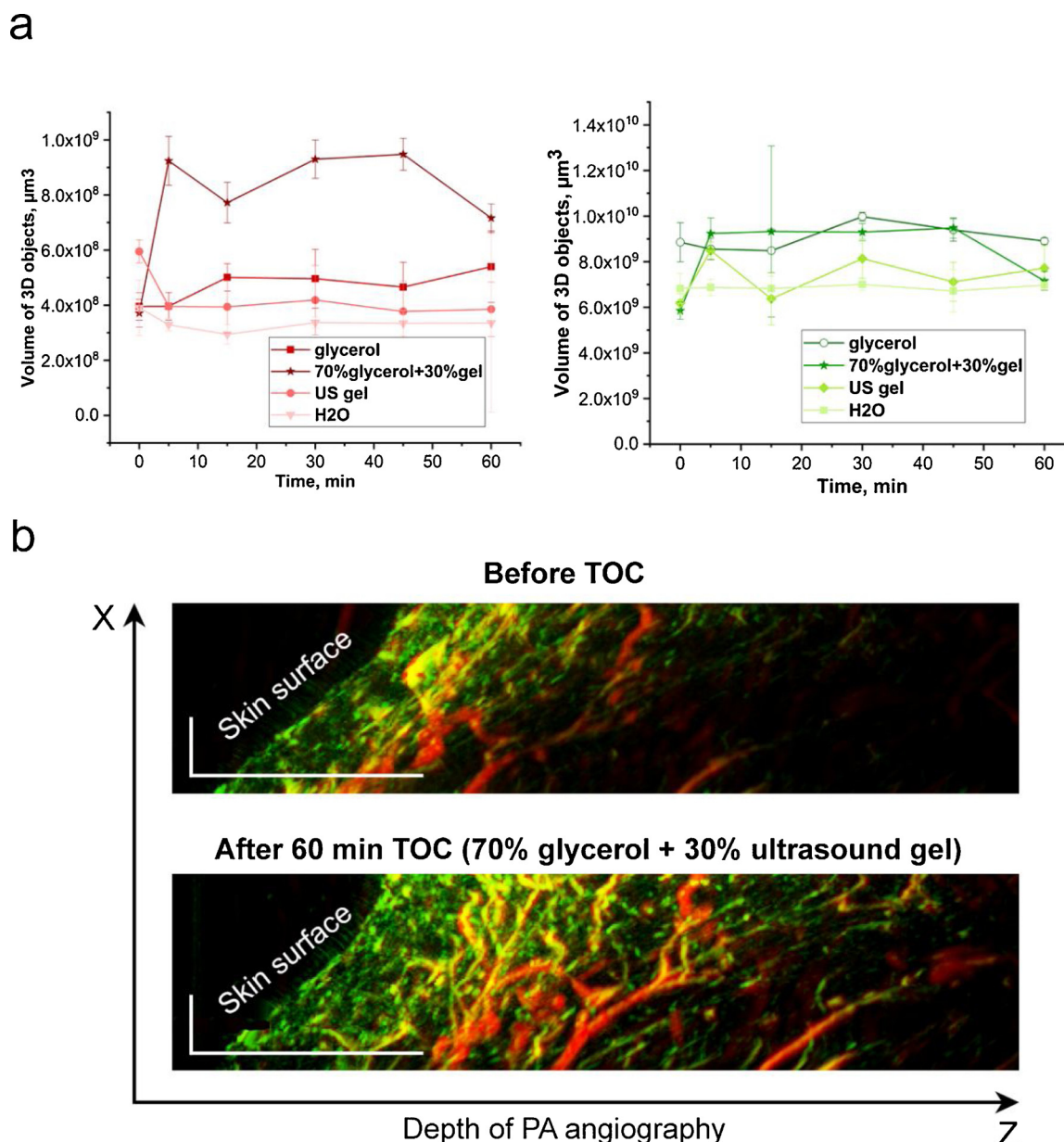
a

b

Fig. 5. *In vivo* effects of RSOM & TOC at the topical application of different OCAs on the skin surface of mouse limb during RSOM imaging procedure. (a) Comparative quantitative analysis (volume of 3D objects) for large (red color signal, left) and small (green color signal, right) vessels at the application of water, US gel, pure glycerol, and mixture of 70 % glycerol + 30 % US gel. (b) PA images (XZ scans) of the same limb area before (conventional RSOM imaging) and after 70 % glycerol + 30 % US gel TOC (RSOM & TOC imaging). Scale bar = 0.5 mm.

4. Conclusions

Our findings, for the first time to our knowledge, demonstrated that RSOM imaging can be significantly improved in depth and quality without prolongation of detection time by integration PAI with TOC in one procedure. Specifically, this can be achieved by using OCA solution instead of water (or US gel) for acoustic coupling during PAI procedure. In preclinical studies *in vivo*, we demonstrated the best RSOM images of mouse limb vascularity after topical application of 70 % glycerol with 30 % US gel between skin surface and transducer. We determined the optimal time interval for RSOM & TOC imaging ranging from 5 to 45 min after OCA exposure to skin. The main advantage of the RSOM & TOC approach is the synergy of two effects that are in demand for PAI: (1) good coupling between transducer and skin for propagation of acoustic signals; and (2) TOC to minimize skin light scattering, which is the main challenge for deep imaging *in vivo*. These benefits together

with using OCA components, which are safe and validated for topical application on human skin, might provide quick clinical translation of PAI with TOC. Specifically, high-resolution 3D RSOM & TOC imaging may be useful for defining interrelation of blood and lymphatic macro- and micro-vessels in local lesions, including diagnosis of vascular disturbances inside of skin pimples, tumors, malformations and nevus. The unique two-phase changes in RSOM images were obtained after intradermal injection of 70 % glycerol (so-called injectable TOC). Highly-improved imaging of superficial small vessels shortly ($\sim$5 min) after injection as a result of skin clearing switched on invisibility of this vascular network due to possible involvement of small vessels in clearing process; and thereby "open a window" for RSOM imaging of deep and relatively large blood vessels. This effect was reversible and lasted $\sim$10-15 min that was enough for RSOM imaging, at least, on small animals. The capability of RSOM imaging was extended by integration of angiography and lymphography, which is important for

diagnosis of lymphedema, venous insufficiency, vascular malformation, cancer and many other diseases. Furthermore, local co-injection of contrast dye for visualization of lymphatic vessels and MNCs as potential drug cargo showed feasibility of using PAI to control targeted lymphatic drug delivery to lymph nodes and drug release there *in vivo*.

It is important that presented approaches can be used not only in RSOM but in any in-house or commercially available PAI platforms for improving diagnosis, prognosis and outcomes of metastatic tumors, malformations, lymphedema and other diseases.

Thus, obtained results open clinically relevant perspectives for deep 3D-PA angio- and lymphography with a potential for PA-controlled targeted lymphatic drug delivery.

Author contributions

V.P.Z., D.A.G, V.V.T. and E.I.G. designed the study; M.V.N. synthetized MNCs; B.N.K. synthetized and provided GNRs; M.V.N., T.O.A., E.I.G., performed the measurements; M.V.N., E.I.G., T.S.Z, D.A.G. and V.P.Z. wrote the manuscript.

Declaration of Competing Interest

Vladimir Zharov, Ekaterina Galanzha, and UAMS have a financial interest in the Technology discussed in this publication. Dr. Vladimir Zharov has a financial interest in CytoAstra, LLC, which has licensed the Technology. These financial interests have been reviewed and approved in accordance with the UAMS conflict of interest policies.

Acknowledgment

Appendix A. Supplementary data

Supplementary material related to this article can be found, in the online version, at doi:https://doi.org/10.1016/j.pacs.2020.100186.

References

[1] V.V. Tuchin, V.P. Zharov, E.I. Galanzha, Biophotonics for lymphatic theranostics in animals and humans, J. Biophotonics 11 (2018) 110–121.
[2] L.L. Munn, T.P. Padera, Imaging the lymphatic system, Microvasc. Res. 96 (2014) 55–63.
[3] A. Khan, J. Mudassir, N. Mohtar, Y. Darwis, Advanced drug delivery to the lymphatic system: lipid-based nanoformulations, Int. J. Nanomedicine 2 (2013) 2733–2744.
[4] G. Mariani, L. Moresco, G. Viale, G. Villa, M. Bagnasco, G. Canavese, J. Buscombe, H.W. Strauss, Radioguided sentinel lymph node biopsy in breast cancer surgery, J. Nucl. Med. 42 (2001) 1198–1215.
[5] G. Mariani, M. Gipponi, L. Moresco, G. Villa, M. Bartolomei, G. Mazzarol, et al., Radioguided sentinel lymph node biopsy in malignant cutaneous melanoma, J. Nucl. Med. 43 (2002) 811–827.
[6] R.Y. Tsien, Imagining imaging's future, Nat. Rev. Mol. Cell Biol. 12 (2003) SS16–SS21.
[7] D.H. O'Leary, J.F. Polak, R.A. Kronmal, T.A. Manolio, G.L. Burke, S.K.Jr. Wolfson, Carotid-artery intima and media thickness as a risk factor for myocardial infarction and stroke in older adults, N. Engl. J. Med. (1999) 14–22.
[8] M. Abbaci, A. Conversano, F. De Leeuw, Laplace-Builhé, Near-infrared fluorescence imaging for the prevention and management of breast cancer-related lymphedema: a systematic review, Eur. J. Surg. Oncol. 45 (2019) 1778–1786.
[9] M. Narushima, T. Yamamoto, F. Ogata, H. Yoshimatsu, M. Mihara, I. Koshima, Indocyanine green lymphography findings in limb lymphedema, J. Reconstr. Microsurg. 32 (2016) 72–79.
[10] J.T. Alander, I. Kaartinen, A. Laakso, T. Pätilä, T. Spillmann, V.V. Tuchin, M. Venermo, P. Välisuo, A review of indocyanine green fluorescent imaging in

[11] surgery, Int. J. Biomed. Imaging 940585 (2012), https://doi.org/10.1155/2012/940585.
[11] E.I. Galanzha, V.P. Zharov, Photoacoustic flow cytometry (review), Methods 57 (2012) 280–296.
[12] E.I. Galanzha, E.V. Shashkov, T. Kelly, J.W. Kim, L. Yang, V.P. Zharov, In vivo magnetic enrichment and multiplex photoacoustic detection of circulating tumour cells, Nat. Nanotechnol. 4 (2009) 855–860.
[13] L.V. Wang, Multiscale photoacoustic microscopy and computed tomography, Nat. Photonics 3 (2009) 503–509.
[14] L.V. Wang, S. Hu, Photoacoustic tomography: in vivo imaging from organelles to organs, Science 335 (80-) (2012) 1458–1462.
[15] S. Mallidi, G.P. Luke, S. Emelianov, Photoacoustic imaging in cancer detection, diagnosis, and treatment guidance, Trends Biotechnol. 29 (2011) 213–221.
[16] D. Razansky, A. Buehler, V. Ntziachristos, Volumetric real-time multispectral optoacoustic tomography of biomarkers, Nat. Protoc. 6 (2011) 1121–1129.
[17] M. Omar, M. Schwarz, D. Soliman, P. Symvoulidis, V. Ntziachristos, Imaging melanin cancer growth in-vivo using raster-scan optoacoustic mesoscopy (RSOM) at 50 MHz and 100 MHz, Photons Plus Ultrasound Imaging Sens. 5 (2016) 97–08.
[18] S. Zackrisson, S.M.W.Y. van de Ven, S.S. Gambhir, Light in and sound out: emerging translational strategies for photoacoustic imaging, Cancer Res. 74 (2014) 979–1004.
[19] V.P. Zharov, E.I. Galanzha, V.V. Tuchin, Photothermal imaging of moving cells in lymph and blood flow in vivo, Proc. SPIE. Int. Soc. Opt. Eng. 2 (2004) 18–25.
[20] E.I. Galanzha, E.V. Shashkov, V.V. Tuchin, V.P. Zharov, In vivo multiparameter multispectral photoacoustic lymph flow cytometry with natural cell focusing, Cytometry 73 (2008) 884–894.
[21] E.I. Galanzha, M.S. Kokoska, E.V. Shashkov, J.W. Kim, V.V. Tuchin, V.P. Zharov, In vivo fiber-based multicolor photoacoustic detection and photothermal purging of metastasis in sentinel lymph nodes targeted by nanoparticles, J. Biophotonics 2 (2009) 528–539.
[22] R. LaComb, O. Nadiarnykh, S. Carey, C.P, Quantitative second harmonic generation imaging and modeling of the optical clearing mechanism in striated muscle and tendon, J. Biomed. Opt. 13 (2008) 13–26.
[23] H. Kajita, K. Kishi, High-resolution imaging of lymphatic vessels with photoacoustic lymphangiography, Radiology 292 (2019) 22–35.
[24] V.V. Tuchin, I.L. Maksimova, D.A. Zimnyakov, I.L. Kon, A.H. Mavlyutov, A.A. Mishin, Light propagation in tissues with controlled optical properties, J. Biomed. Opt. 2 (1997) 401–417.
[25] E.I. Galanzha, V.V. Tuchin, Q. Luo, H. Cheng, A.V. Solov'eva, The action of osmotically active drugs on optical properties of skin and state of microcirculation in experiments, Asian J. Phys. 10 (2001) 1–15.
[26] V.P. Zharov, E.I. Galanzha, E.V. Shashkov, N.G. Khlebtsov, V. Tuchin, In vivo photoacoustic flow cytometry for monitoring of circulating single cancer cells and contrast agents, Opt. Lett. 31 (2006) 3623–3625.
[27] D. Zhu, K.V. Larin, Q. Luo, V. Tuchin, A Recent progress in tissue optical clearing, Laser Photon, Rev. 7 (2013) 732–757.
[28] Y.A. Menyaev, D.A. Nedosekin, M. Sarimollaoglu, M.A. Juratli, E.I. Galanzha, V.V. Tuchin, V.P. Zharov, Optical clearing in photoacoustic flow cytometry, Biomed. Opt. Exp 4 (2013) 3030–3041.
[29] J. Seo, M. Choe, S.Y. Kim, Clearing and labeling techniques for large-scale biological tissues, Mol. Cells 39 (2016) 439–446.
[30] A. Liopo, R. Su, D.A. Tsyboulski, A.A. Oraevsky, Optical clearing of skin enhanced with hyaluronic acid for increased contrast of optoacoustic imaging, J. Biomed. Opt. 21 (2016) 11–21.
[31] E. Song, H. Seo, K. Choe, Y. Hwang, J. Ahn, S. Ahn, P. Kim, Optical clearing based cellular-level 3D visualization of intact lymph node cortex, Biomed. Opt. Exp. 6 (2015) 4154–4164.
[32] Z.1 Mao, D. Zhu, Y. Hu, X. Wen, Z. Han, Influence of alcohols on the optical clearing effect of skin in vitro, J. Biomed. Opt. 13 (2008) 125–136.
[33] X. Yang, Y. Liu, D. Zhu, R. Shi, Q. Luo, Dynamic monitoring of optical clearing of skin using photoacoustic microscopy and ultrasonography, Opt. Express. 22 (2014) 80–94.
[34] Y. Liu, X. Yang, D. Zhu, R. Shi, Q. Luo, Optical clearing agents improve photoacoustic imaging in the optical diffusive regime, Opt. Lett. 38 (2013) 423–426.
[35] R. Shi, L. Guo, C. Zhang, W. Feng, P. Li, Z. Ding, D. Zhu, A useful way to develop effective in vivo skin optical clearing agents, J. Biophotonics 10 (2017) 887–895.
[36] Jing Wang, Ning Ma, Rui Shi, Yang Zhang, Tingting Yu, D. Zhu, Sugar-induced skin optical clearing: from molecular dynamics simulation to experimental demonstration, IEEE J. Sel. Top. Quantum Electron. 20 (2014) 12–34.
[37] W. Feng, R. Shi, N. Ma, D.K. Tuchina, V.V. Tuchin, D. Zhu, Skin optical clearing potential of disaccharides, J. Biomed. Opt. 21 (2016) 081207.
[38] V.V. Tuchin, Optical Clearing of Tissues and Blood, (2006).
[39] R. Barer, Spectrophotometry of clarified cell suspensions, Science 121 (80-) (1955) 709–715.
[40] D.W. Leonard, K.M. Meek, Refractive indices of the collagen fibrils and extrafibrillar material of the corneal stroma, Biophys. J. 72 (1997) 1382–1387.
[41] M.V. Novoselova, D.N. Bratashov, M. Sarimollaoglu, D.A. Nedosekin, W. Harrington, A. Watts, M. Han, B.N. Khlebtsov, E.I. Galanzha, D.A. Gorin, V.P. Zharov, Photoacoustic and fluorescent effects in multilayer plasmon-dye interfaces, J. Biophotonics 12 (2018) 12–24.
[42] N.G. Khlebtsov, Determination of size and concentration of gold nanoparticles from extinction spectra, Anal. Chem. 80 (2008) 6620–6625.
[43] Yu. Yanina, N.A. Navolokin, Yu.I. Svenskaya, A.B. Bucharskaya, G.N. Maslyakova, D.A. Gorin, G.B. Sukhorukov, V.V.T. Morphology, alterations of skin and subcutaneous fat at NIR laser irradiation combined with delivery of encapsulated indocyanine green, J. Biomed. Opt. (2017) 22.

[44] E.S. Tuchina, V.V. Tuchin, B.N. Khlebtsov, N.G. Khlebtsov, Phototoxic effect of conjugates of plasmon-resonance nanoparticles with indocyanine green dye on Staphylococcus aureus induced by IR laser radiation, Quantum Electron. 41 (2011) 354–359.

[45] H. Kajita, A. Oh, M. Urano, M. Takemaru, N. Imanishi, M. Otaki, T. Yagi, S. Ais, K. Kishi, Photoacoustic lymphangiography, J. Surg. Oncol. 2 (2019) 4–11.

[46] Byung-Boong Lee, Stanley G. Rockson, J.B. Lymphedema, A Concise Compendium of Theory and Practice, (2018).

[47] B. Sarri, X. Chen, R. Canonge, S. Grégoire, F. Formanek, J.B. Galey, A. Potter, T. Bornschlögl, H. Rigneault, In vivo quantitative molecular absorption of glycerol in human skin using coherent anti-Stokes Raman scattering (CARS) and two-photon auto-fluorescence, J. Control. Release 308 (2019) 190–196.

[48] E.I. Galanzha, V.V. Tuchin, A.V. Soloviva, T.V. Stepanova, O. Luo, H. Cheng, Skin backreflectance and microvascular system functioning at the action of osmotic agents, J. Phys. D. Appl. Phys. 36 (2003) 17–39.

[49] E. Youn, T. Son, H.-S. Kim, B. Jung, Determination of optimal glycerol concentration for optical tissue clearing, Photonic Ther. Diagn. (2012) 8207.
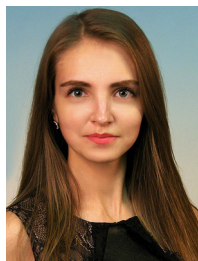
Marina Novoselova is the Research Scientist at the Biophotonic laboratory, Skolkovo Institute of Science and Technologies. She received the Ph.D. in engineering science (2016). Marina Novoselova has more than 6 years of research experience in the fields of bionanotechnology and material sciences. Her current interests are targeted therapeutics and magnetic drug delivery and developing of contrast agents for fluorescent and photoacoustic imaging.

Tatiana Abakumova graduated from Pirogov Russian National Research Medical University in 2012. In January 2016 she got a Ph.D. in biochemistry with thesis «Targeted systems for MRI visualization of brain pathologies». From May 2016 to December 2018 she worked as a Senior Research Scientist in immunochemistry laboratory in the same department. Her research interests linked with targeted delivery of therapeutic and diagnostic agents to the tumor cells using different drug delivery systems (nanogels, liposomes or micelles). Tatiana Abakumova has a number of awards for her oral and poster presentations on the international conferences. She got scholarships from the Government of Russian Federation, funds and grants from different funds to support own research. She published 17 papers and 30 conference abstracts.

Boris Khlebtsov (b. 1980), Senior scientist at Laboratory of Nanobiotechnology at the Institute of Biochemistry and Physiology of Plants and Microorganisms, Russian Academy of Sciences (IBPPM RAS). Degrees: Doctor of Physical and Mathematical Sciences (habilitation), Specialty - Biophysics, Saratov State University (2011). Field of Research and Experience: Synthesis, simulation and application of noble metal nanoparticles. Static and dynamic light scattering by small particles, optics of disperse systems, thermodynamics of high polymer solutions, Fortran programming and calculation of light scattering and absorption by using various approximate and state-of-art methods. Publications: more than 150 scientific papers published in international scientific journals and books.

Timofei Zatsepin is an Associate Professor at the Center of Life Sciences, Skolkovo Institute of Science and Technology (Moscow, Russia). He has received MS in Chemistry in 2000 and PhD degree in Bioorganic Chemistry Chemistry in 2003 from Moscow State University. Timofei first joined Skoltech in 2013 as Associate Director of the Center for Functional Genomics. Timofei is a strong scholar and entrepreneur with a solid background in oligonucleotides synthesis and applications *in vitro* and *in vivo* awarded by Academia Europea Prize. Research interests of Prof. Zatsepin are in RNA therapeutics and oligonucleotides for *in vitro* diagnostics.
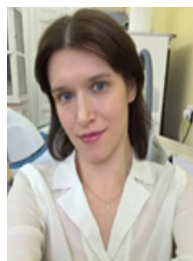
Ekaterina N. Lazareva received her MS degree from Saratov State University, Department of Optics and Biophotonics where currently she is a PhD student and an Engineer. Her research interests are in optical properties of biological tissues, especially of blood (its components) and adipose tissue, refractometry and spectroscopy of tissues, and tissue optical clearing.

Valery V. Tuchin is a professor and chair of Optics and Biophotonics at Saratov State University. He is also the head of Laboratory of Laser Diagnostics of Technical and Living Systems, Institute of Precision Mechanics and Control of the RAS, and the supervisor of Interdisciplinary Laboratory of Biophotonics at Tomsk State University and Laboratory of FemtoMedicine of ITMO University. His research interests include tissue optics, laser medicine, tissue optical clearing, and nanobiophotonics. He is a member of SPIE, OSA, and IEEE, Guest Professor of HUST and Tianjin Universities, and Adjunct Professor of the Limerick University and National University of Ireland. He has published more than 700 papers, 27 monographs and textbooks, and 58 book chapters. Dr. Tuchin is also a holder of more than 50 patents. His works were cited more than 25,000 times.

Vladimir P. Zharov is the director of the Arkansas Nanomedicine Center, a Professor of Biomedical Engineering (BME) and Josephine T. McGill Chair in Cancer Research at the University of Arkansas for Medical Sciences (UAMS). He is the author of 5 books, 55 patents, and more than 200 papers in the field of laser spectroscopy, biophotonics, and nanomedicine including 10 publications in the Nature journals. He is one of the pioneers of high resolution photoacoustic spectroscopy and the inventor of photoacoustic tweezers, nanobubble-based theranostics cancer and infections, *in vivo* multicolor flow cytometry and biomedical application of spaser as smallest (20 nm) plasmonic nanolaser. His laser-based technologies have been commercialized and broadly used in clinics. Dr. Zharov is the State Prize Winner in Russia, the most prestigious national award in Russia, and the first recipient of the U.S. Maiman Award named after the inventor of the first laser.

Dmitry Gorin is a professor at the Skoltech center of Photonics & Quantum Materials (CPQM) at Skoltech Institute of Science and Technology (Moscow, Russia) and head of Biophotonics Lab. He has received Diploma of Engineer-Physicist in 1997 and his CSc (PhD) degree and his DSc degree in Physical Chemistry in 2001 and 2011 from Saratov State University, respectively. He was a PostDoc fellow in the Max Planck Institute of Colloids and Interfaces. He is author and co-author of 135 articles in peer-reviewed journals, 1 book and 5 book chapter and 8 tutorials for students and PhD students, and co-inventor of 15 patents. Research interests of Prof. Gorin are in Biophysics, Biophotonics, Theranostics, Physics and Chemistry of Colloids and Interfaces.

Ekaterina I. Galanzha heads the Laboratory of Lymphatic Research, Diagnosis and Therapy (LDT) at the University of Arkansas for Medical Sciences, USA. She published > 60 peer-reviewed manuscripts and 5 book chapters. She is a co-inventor of the *in vivo* lymph flow cytometry. Based on her medical background, extensive experience in the lymphatic research and interdisciplinary skills in photoacoustics, nanomedicine and biophotonics, she and her laboratory pursue the goal to use advanced technical approaches for discovering lymphatic-related mechanisms of human diseases and translating obtained knowledge into clinics.